Drug Design, Development and Therapy

Dovepress
open access to scientific and medical research

Open Access Full Text Article

ORIGINAL RESEARCH

Exosomes Derived from MicroRNA-146a-5p-Enriched Bone Marrow Mesenchymal Stem Cells Alleviate Intracerebral Hemorrhage by Inhibiting Neuronal Apoptosis and Microglial M1 Polarization

This article was published in the following Dove Press journal:
Drug Design, Development and Therapy

Shurong Duan
Fei Wang
Jingwei Cao
Chunyan Wang

Department of Neurology, The First Affiliated Hospital of Harbin Medical University, Harbin 150001, People's Republic of China

Introduction: Intracerebral hemorrhage (ICH) is a devastating type of stroke with high mortality, and the effective therapies for ICH remain to be explored. Exosomes (Exos) have been found to play important roles in cell communication by transferring molecules, including microRNAs (miRNAs/miRs). MiRNAs are critical regulators of genes involved in many various biological processes and have been demonstrated to aggravate or alleviate brain damages induced by ICH. The aim of the present study was to investigate the effect of Exos derived from miR-146a-5p-enriched bone marrow mesenchymal stem cells (BMSCs-miR-146a-5p-Exos) on experimental ICH.

Methods: ICH was induced in adult male Sprague-Dawley rats by an intrastriatal injection of collagenase type IV. At 24 h after surgery, Exos were administrated. For detecting apoptotic cells, TUNEL staining was performed using an in situ Cell Death Detection Kit. Fluoro-Jade B staining was performed to detect degenerating neurons. Immunofluorescence assay was performed to detect the expression of myeloperoxidase (MPO) and OX-42. The binding of miR-146a-5p and its target genes was confirmed by luciferase reporter assay.

Results: At 24 h after surgery, BMSCs-miR-146a-5p-Exos administration significantly improved neurological function, reduced apoptotic and degenerative neurons, and inhibited inflammatory response. Furthermore, miR-146a-5p-enriched Exos obviously inhibited the M1 polarization of microglia after ICH in rats, accompanied by the reduced expression of pro-inflammatory mediators releasing by M1 microglia including inducible nitric oxide synthase (iNOS), cyclooxygenase-2 (COX-2) and monocyte chemoattractant protein-1 (MCP-1). Finally, we observed that miR-146a-5p directly targeted interleukin-1 receptor-associated kinase1 (IRAK1) and nuclear factor of activated T cells 5 (NFAT5), which contributed to the inflammation response and the polarization of M1 microglia/macrophages.

Conclusion: We demonstrated that miR-146a-5p-riched BMSCs-Exos could offer neuroprotection and functional improvements after ICH through reducing neuronal apoptosis, and inflammation associated with the inhibition of microglial M1 polarization by downregulating the expression of IRAK1 and NFAT5.

Keywords: intracerebral hemorrhage, microRNA-146a-5p, exosomes, apoptosis, microglial M1 polarization

Correspondence: Chunyan Wang
Department of Neurology,
The First Affiliated Hospital of Harbin Medical University, 23 Youzheng Street, Harbin 150001, People's Republic of China
Tel/Fax +86-451-85555130
Email wxqsjnk1@163.com

Introduction

Intracerebral hemorrhage (ICH) is a severe type of stroke with high mortality and morbidity, accounting for 15% of the total stroke-related cases.[1] Cerebral edema and neuroinflammation after ICH cause a series of secondary injuries, thus leading to

severe neurological defects.[2] There is currently no effective treatment for ICH and ICH-induced secondary brain injuries. New alternate candidates need to be developed to prevent neurological deterioration after ICH.

Microglia, the macrophages exist in the brain, originate from yolk-sac-derived erythromyeloid progenitor cells and subsequently migrate into the brain and populate the brain rudiment early during development.[3] Microglia have been suggested to be involved in the neuronal proliferation, neuronal differentiation, synaptic formation and neuroinflammation.[4,5] Emerging data have showed that microglia have two different polarization statuses, M1 and M2 phenotypes.[6] M1 phenotype microglia mainly secret pro-inflammatory cytokines inducible nitric oxide synthase (iNOS), tumor necrosis factor (TNF)-α, interleukin (IL)-6, and monocyte chemoattractant protein-1 (MCP-1) promoting neuroinflammation, while M2 polarized microglia inhibit neuroinflammatory response. Studies have shown that the reduction in microglial M1 polarization protects hemorrhagic brain after ICH.[7,8]

Exosomes (Exos) are small nanosized membranous vesicles with a 30–100 nm diameter released from diverse cell types and transfer biomolecules, including microRNAs (miRNAs/miRs), long noncoding RNAs (lncRNAs) and proteins. They are thought to play important roles in various biological progresses such as cell-to-cell communication, tumor progression, antigen presentation, and cellular waste disposal.[9] An extensive body of recent researches has revealed that bone marrow-derived mesenchymal stem cells (BMSCs) release Exos that can improve various diseases.[10,11] Recently, neurovascular remodeling and functional recovery involving MSC-derived Exos have also been implicated in the progress of ICH.[12]

MiRNAs are small endogenous RNAs that regulate gene expression at the post-transcriptional level. Rapidly accumulating evidences have indicated that miRNAs are crucial regulators in ICH.[13,14] Exosomal miRNAs expression varies widely in different cell types and pathological states, and miR-modified Exos may alter its function. MiR-146a-5p is highly conserved among humans, mice, and rats. Recent researches also have showed that miR-146a-5p is abundant in MSCs, and stimulatory effects of human umbilical cord MSC-Exos on primordial follicles are through carrying functional miR-146a-5p.[15,16] The beneficial functions exert by Exos may be related to the high level of miR-146a-5p it carries. Many studies have shown that miR-146a protects against various brain impairments.[17–19] It is also involved in the modulation of microglia/macrophages in ischemic stroke.[20] In addition, miR-146a-5p has been reported to be down-regulated in the serum of patients with ICH[21] and to protect against ICH by repressing the TRAF6/NF-κB pathway.[19] However, the specific mechanism of miR-146a-5p on the neuroprotection after ICH remains to be clarified.

Considering the crucial role of MSCs-Exos in ICH and the potential function of miR-146a-5p on neurological impairment associated with brain injury, the present study focused on investigating whether miR-146a-5p-enriched Exos derived from BMSCs could contribute to the neuroprotective effects on ICH and the possible molecular mechanisms involved in this process.

Materials and Methods

Isolation and Identification of BMSCs

All animal experiments were performed in accordance with the Guideline for the Care and Use of Laboratory Animals published by the National Institutes of Health and the Ethics Committee of the First Affiliated Hospital of Harbin Medical University. BMSCs were isolated as previously described.[22,23] Briefly, BM was harvested by flushing isolated from tibia and femur of healthy rats with DMEM medium (D5648, Sigma, Saint Louis, MO, USA) under sterile conditions. The obtained cell suspense was centrifuged and incubated with red blood cell lysis buffer (R1010, Solarbio, Beijing, China) to deplete the red blood cells. Then, the cells were suspended and cultured at 37°C with 5% CO_2. After washing with PBS, BMSCs were cultured in DMEM supplemented with 10% fetal bovine serum (FBS).

For the identification of BMSCs,[24] the immunophenotype of isolated BMSCs was examined by flow cytometry. BMSCs were negative for the hematopoietic marker CD34 and CD45, while strongly positive for MSC-specific markers including CD29 and CD90. Adipogenic and osteogenic differentiation assays were performed for the multi-differentiation of BMSCs. BMSCs were incubated into adipogenic or osteogenic chondrogenic differentiation medium for 21 days. Then, the cells were fixed and stained with Oil Red O (G1262, Solarbio) or Alizarin Red (G1450, Solarbio), respectively.

Transfection of BMSCs

MiR-146a-5p was transfected into the BMSCs via the lentiviral vector (LV)-mediated method. BMSCs (1×10^5) were plated and transfected with LV-miR-146a-5p or empty vector at a multiplicity of infection (MOI) of 20. BMSCs were infected by the appropriate volume of virus solution then incubated at 37°C, 5% CO_2 overnight. After that, the culture medium containing lentivirus was replaced with DMEM

medium containing 10% FBS, and the incubation was continued for 24 h for subsequent detection.

Isolation and Identification of Exos Derived from BMSCs

Culture supernatants of BMSCs infected with LV-miR-146a-5p or LV were centrifuged for 30 minutes at 2000 × g. Exos pellets were then obtained from the purified supernatants using the Total Exosome Isolation reagent (4,478,359, Thermo Fisher Scientific, Waltham, MA, USA) according to the manufacturer's instructions. Subsequently, Exos were collected, ultracentrifuged at 10,000 × g for 1 h at 4°C and resuspended in PBS. Finally, the ultrastructural morphology of Exos was identified using an electron microscope.

ICH Model and MiR-146a-5p Administration

Adult male Sprague-Dawley (SD) rats (8–9 weeks old) obtained from Beijing Huafukang Biotechnology Co., Ltd. (Beijing, China) were subjected to ICH/Sham. ICH was induced in the rat by an intrastriatal injection of collagenase type IV. After rats were anesthetized, a 1-mm burr hole was drilled using dental drill (stereotaxic coordinates: 0.5 mm posterior to the bregma, 4.5 mm right of the middle line and 6 mm deep from the skull surface). Collagenase IV (0.5 U in 1 μL saline) was infused into the brain at a flow rate of 0.2 μL/min. For the rats in Sham group, an equal volume of saline was infused into the striatum through a burr hole drilled in the same position. At 24 h after ICH induction, BMSCs-Exos (100 μg/mL, 100 μg) or BMSCs-miR-146a-5p-Exos (100 μg/mL, 100 μg) or equivalent amount of normal saline was administered via the tail vein. Some rats were sacrificed 24 h after Exos administration for histological and molecular studies. The remaining rats were fed for behavioral tests at 1 d, 7 d and 28 d after Exos administration. Rats with the ICH surgery showed a 30% mortality. Rats with ICH surgery that did not exhibit obvious neurological defects were excluded from this study.

Behavioral Tests

Behavioral tests, including beam walking test and motor deficit score, were performed at 1 d, 7 d and 28 d after Exos administration.

The motor deficit score was evaluated by observation of spontaneous ipsilateral circling, contralateral hindlimb retraction, beam walking ability and bilateral forepaw grasp, as previously described.[25] The specific tests as following: (1) observation of spontaneous ipsilateral circling, graded from 0 (no circling) to 3 (continuous circling); (2) contralateral hindlimb retraction, which measured the ability of the animal to replace the hindlimb after it was displaced laterally by 2 cm to 3 cm, graded from 0 (immediate replacement) to 3 (replacement after minutes or no replacement); (3) beam walking ability, which was graded 0 for a rat that readily traversed a 2.4 cm wide, 80 cm long beam to 3 for a rat unable to stay on the beam for 10 s; and (4) bilateral forepaw grasp, which measured the ability of the rat to hold onto a 2-mm diameter steel rod, graded 0 for a rat with normal forepaw grasping behavior to 3 for a rat unable to grasp with the forepaws.

The Beam Walking test evaluated the ability of the rats to walk along a wooden beam, and scores were assigned using methods previously described.[25] Performance was rated on a 7 point scale: (1) the rat is unable to place the affected hindlimb on the horizontal surface of the beam; (2) the rat places the limb on the beam and maintains balance but is unable to traverse the beam; (3) the rat traverses the beam dragging the affected hindlimb; (4) the rate traverses the beam and places the affected hindlimb on the horizontal surface of the beam once; (5) the rat crosses the beam and places the affected hindlimb on the horizontal surface of the beam to aid during less than half of the steps; (6) the rat uses the affected hindlimb to aid in more than half of the steps; and (7) the rat traverses the beam with no more than two foot slips.

Distribution of Exos in Hemorrhage Region

The ICH model was carried out as detailed before. Then, DiI-labeled Exos were injected into ICH rats. At 24 h after injection, the rats were sacrificed. Brain tissue was fixed, dehydrated and cut into 10 μm sections. After washing with PBS, a fluorescence microscope (BX53, Olympus, Tokyo, Japan) was used to detect the distribution of Exos in the brain tissue of rats.

TUNEL Staining

For detecting apoptotic cells, TUNEL staining was performed using an in situ Cell Death Detection Kit (11,684,817,910, Roche, Basel, Switzerland). Deparaffinized brain sections were permeabilized with Triton X-100 (ST795, Beyotime, Shanghai, China) and were incubated with the TUNEL reaction mix at 37°C for 60 min. After incubation with NeuN-neuronal marker (1:200 dilution, ab104224, Abcam, Cambridge, MA, USA) at 4°C overnight, the sections were incubated with the corresponding secondary antibody (1:200

dilution, A0521, Beyotime) at 37°C for 60 min. Finally, TUNEL-positive neurons were observed under a fluorescence microscope (BX53, Olympus).

Fluoro-Jade B (FJB) Staining

FJB staining was performed to detect degenerating neurons. Brain sections were deparaffinized, rehydrated, and transferred to a solution of 0.06% potassium permanganate for 10 min. The sections were then rinsed in distilled water for 2 min and stained with FJB (AG310-30MG, Merckmillipore, Bedford, MA, USA) for 20 min in the dark. Subsequently, the stained slides were thoroughly washed with distilled water, dried and coverslipped. FJB-positive neurons were counted under a fluorescence microscope (BX53, Olympus).

Immunofluorescence Assay

For immunofluorescence, deparaffinized brain sections were blocked for 15 min in goat serum. After incubation with primary antibodies anti-MPO (1:100 dilution; ab9535, Abcam), anti-OX42 (1:100 dilution; ab1211, Abcam) or co-incubation with anti-MHC-II (1:200 dilution; ab23990, Abcam) and Iba-1 (1:200 dilution; ab178847, Abcam) at 4°C overnight, the sections were incubated with the corresponding secondary antibody (1:200 dilution, A0562, A0516 or A0521, Beyotime) at 37°C for 60 min and mounted with 4,6-diamidino-2-phenylindole (DAPI, D106471-5mg, Aladdin, Shanghai, China). The pictures were captured using a fluorescence microscope (BX53, Olympus).

Detection of Pro-Inflammatory Cytokines and Oxidative Stress Markers

The levels of pro-inflammatory cytokines, tumor necrosis factor (TNF)-α, IL-6 and interleukin (IL)-1β in brain tissues were determined by commercial detection kits purchased from USCN Life Science Inc., (TNF-α, SEA133Ra; IL-6, SEA079Ra; IL-1β, SEA563Ra; Wuhan, China) according to the manufacturer's instructions.

The levels of oxidative stress markers malondialdehyde (MDA) and superoxide dismutase (SOD) in brain tissues were determined by commercial detection kits purchased from Nanjing Jiancheng Bioengineering Institute (MDA, A003-1; SOD, A001-1; Nanjing, China) according to the manufacturer's instructions.

Quantitative Real-Time PCR (qRT-PCR)

qRT-PCR was performed for the detection of miR-146a-5p expression in the BMSCs and brain tissues. Total RNAs were extracted using TriPure Reagent (RP1001, BioTeke, Beijing, China). RNA concentration was determined using an ultraviolet spectrophotometer NANO 2000 (Thermo Fisher Scientific, MA, USA). For reverse transcription, miR-146a-5p was extended with a specific loop primer, 5′-GTTGGCTCTGGTGCAGGGTCCGAGGTATTCGCAC-CAGAGCCAACAACCCA-3′ by super M-MLV reverse transcriptase (PR6502, BioTeke). Thereafter, qRT-PCR was performed using Master Mix (PR1702, BioTeke) and SYBR Green I (S9430, Sigma), and was fulfilled with an Exicycler 96 Quantitative PCR Analyzer (Bioneer, Daejeon, Korea). U6 was quantified as an internal RNA control. The following primers were used: miR-146a-5p, forward 5′-GGCCTGAGAACTGAATTCCATGG-3′, reverse 5′-GTGCAGGGTCCGAGGTATTC-3′; U6, forward 5′-GATCTCGGAAGCTAAGCAGG-3′, reverse 5′-TGGTGCAGGGTCCGAGGTAT-3′.

iNOS, forward 5′-TTGGAGCGAGTTGTGGATTG-3′, reverse 5′-GTGAGGGCTTGCCTGAGTGA-3′; COX2 forward 5′- GAACACGGACTTGCTCACTT-3′, reverse 5′-ACGATGTGTAAGGTTTCAGG-3′;

MCP-1, forward 5′-TGGGTCCAGAAGTACATTAGA-3′, reverse 5′- GGGTCAAGTTCACATTCAAAG-3′; β-actin forward 5′- GGAGATTACTGCCCTGGCTCCTAGC-3′, reverse 5′- GGCCGGACTCATCGTACTCCTGCTT-3′. All PCR primers were synthesized by GenScript Biotechnology Co., Ltd (Nanjing, China).

Western Blot Analysis

Proteins were extracted from BMSCs or brain tissues with RIPA lysis buffer (P0013, Beyotime) and separated by SDS polyacrylamide gel electrophoresis (P0015, Beyotime). Then, the separated proteins were transferred onto polyvinylidene fluoride (PVDF) membranes (IPVH00010, Millipore, Bedford, MA, USA). After blocked with 5% skim milk, the PVDF membranes were incubated with the primary antibodies, including CD63 (1:1000 dilution, A5271, ABclonal, Wuhan, China), CD9 (1:1000 dilution, A10789, ABclonal), CD81 (1:700 dilution, Ab109201, Abcam), interleukin-1 receptor-associated kinase1 (IRAK1, 10,478-1-AP, 1:1000 dilution, Proteintech, Wuhan, China), nuclear factors of activated T-cells 5 (NFAT5, 1:1000 dilution, bs-9473R, Bioss, Beijing, China) at 4°C overnight. The next day, the membranes were incubated with the corresponding secondary antibody at room temperature for 1 h. The proteins were visualized using the enhanced chemiluminescence substrate (ECL, P0018, Beyotime), and analyzed by Gel-Pro Analyzer

software (Media Cybernetics, Rockville, MD, USA). The β-actin protein served as an internal control.

Dual-Luciferase Reporter Assay

Wild-type (WT) 3′untranslated region (UTR) containing the predicted miR-146a-5p targeting sites, or corresponding mutant (MUT) 3′-UTR of IRAK and NFAT5 wild-type was inserted into the pmirGLO vector, respectively. Next, 293T cells were co-transfected with these luciferase reporter vectors and miR-146a-5p/NC mimic. Forty-eight hours after transfection, relative (Firefly/Renilla) luciferase activity was determined using a Dual-Luciferase Reporter Assay kit (E1910, Promega, Madison, USA).

Statistical Analysis

The data of beam walking and motor deficit test was presented as median and the data were compared using the Kruskal–Wallis test followed by Dunn's post hoc test. Other data were expressed as mean ± standard deviation (SD) and were compared using One-way ANOVA and Tukey's post hoc test. GraphPad Prism 8.0.1 software (GraphPad Software Inc., La Jolla, CA, USA) was used for statistical analysis. A P value less than 0.05 was considered statistically significant.

Results

Isolation and Characterization of BMSCs

Immuno-phenotypes of isolated BMSCs were analyzed by flow cytometry. Results revealed that BMSCs were positive for MSC-specific markers including CD29 and CD90, while negative for the hematopoietic marker CD34 and CD45 (Figure 1A).

The differentiation of BMSCs into osteogenic and adipogenic was verified using Alizarin Red and Oil Red O staining. When BMSCs were cultured in osteogenic differentiation medium, some of the cells differentiated into mature osteogenic cells that positively stained with Alizarin Red (Figure 1B). When BMSCs were cultured in adipogenic differentiation medium, some of the cells differentiated into mature adipocytes that positively stained with Oil Red O (Figure 1C).

The BMSCs were infected by constructed lentivirus to overexpress miR-146a-5p. qRT-PCR analysis after lentivirus infection to BMSCs demonstrated that LV-miR-146a-5p significantly increased miR-146a-5p expression compared to control (Figure 1D).

Isolation and Characterization of BMSCs-Exos

Electron microscopy revealed that BMSCs-Exos exhibited a cup-shaped or round-shaped morphology (Figure 2A). Next, we examined whether extracellular miRNAs are located within Exos secreted from LV-infected BMSCs. The expression level of miR-146a-5p was assayed by qRT-PCR. Results showed that the expression level of miR-146a-5p was significantly upregulated in Exos derived from miR-146a-5p-overexpressed BMSCs (Figure 2B).

Western blot analysis of the protein expression of some exosomal markers including CD9, CD63 and CD81 further identified the Exos (Figure 2C–E).

Effect of BMSCs-MiR-146a-5p-Exos on Behavior of Rats with ICH

To evaluate the protective effect of BMSCs-miR-146a-5p-Exos on the recovery of neurological function, beam-walking score and motor deficit score were assessed at day 1, 7 and 28 post Exos administration. In terms of the beam-walking score, rats in the ICH group had obviously decreased scores compared with the Sham rats on days 1, 7 and 28 after treatment, while this decrease was significantly inhibited by BMSCs-miR-146a-5p-Exos administration at day 7 and 28 after treatment (Figure 3A). Results showed that the ICH rats had a greater motor deficit score compared with the sham rats; however, BMSCs-miR-146a-5p-Exos administration significantly reduced ICH-induced motor deficit on days 7 and 28 post Exos administration (Figure 3B). Additionally, the effect of BMSCs-miR-146a-5p-Exos on improved beam-walking score and motor deficit score was stronger than the BMSCs-Exos group. We then observed Exos distribution, and abundant Exos were showed in the injured brain region of ICH rats injected with DiI-labeled Exos (Supplemental Figure S1)

Effect of BMSCs-MiR-146a-5p-Exos on Neuronal Apoptosis Following ICH

The neuronal neurodegeneration and apoptosis were detected using FJB and TUNEL staining, respectively. FJB-positive cells were significantly increased in the brain tissue of rats with ICH than that in the Sham group. However, this increase was significantly inhibited by the administration with BMSCs-miR-146a-5p-Exos. BMSCs-Exos also attenuated neuronal neurodegeneration, though its effect on improving neurodegeneration was not as strong as that of

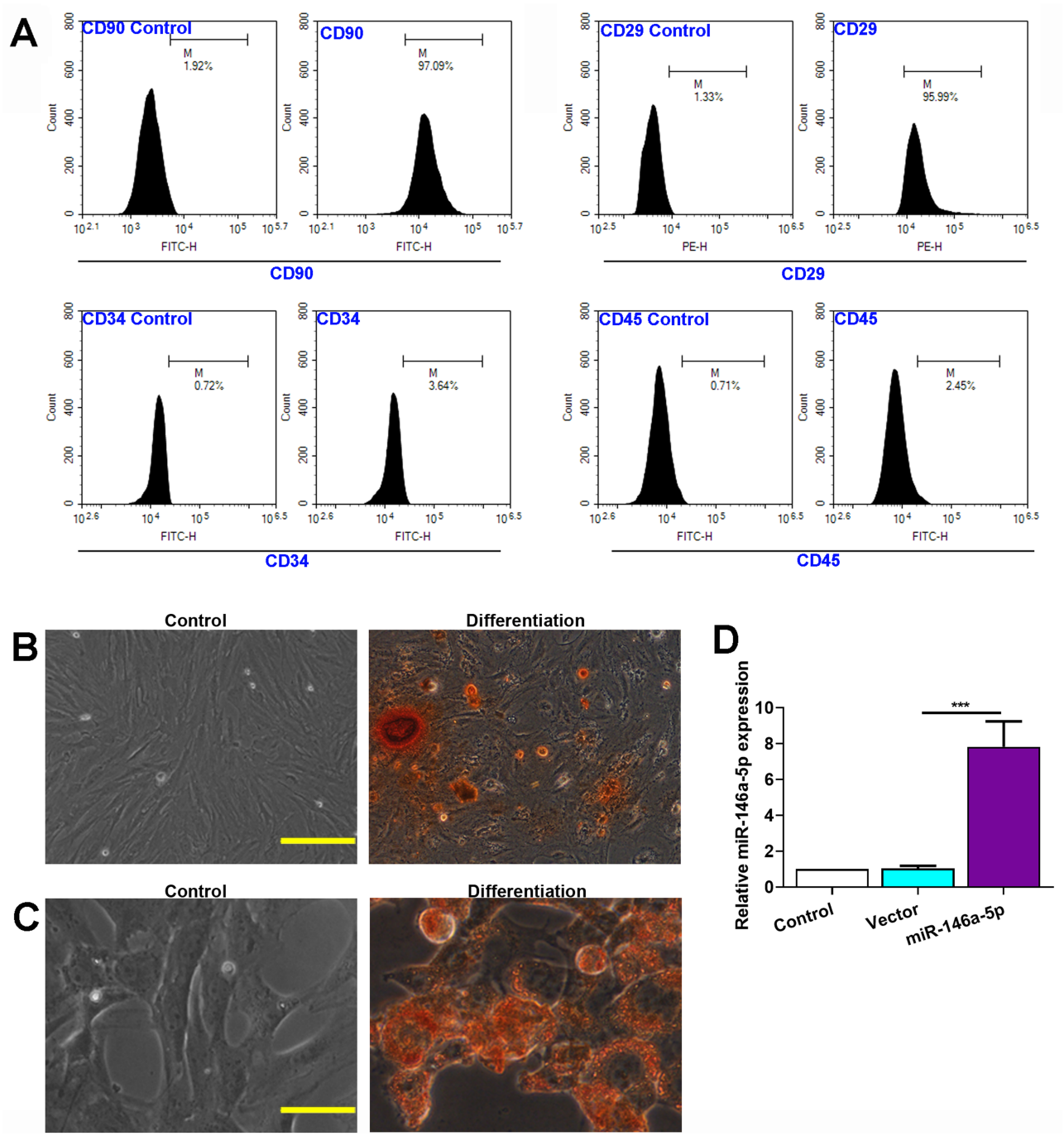

Figure 1 Characterization of BMSCs. (**A**) Flow cytometry analysis of BMSCs surface markers CD90, CD29, CD34 and CD45. Proper isotype was used as control. (**B**) Osteogenic differentiation of BMSCs, scale bar=100 μm. (**C**) Adipogenic differentiation of BMSCs, scale bar=50 μm. (**D**) Expression level of miR-146a-5p in BMSCs infected with LV-miR-146a-5p or LV-vector. The data are presented as the mean ± SD, ***p < 0.001.

miR-146a-5p-enriched Exos (Figure 3C and D). Similar results were also observed in TUNEL assay, BMSCs-miR-146a-5p-Exos or BMSCs-Exos administration significantly reduced neuronal apoptosis induced by ICH, and miR-146a-5p-enriched Exos derived from BMSCs has stronger protective effects than BMSCs-Exos (Figure 3E and F).

Effect of BMSCs-MiR-146a-5p-Exos on Oxidative Stress and Inflammation Following ICH

To evaluate the states of oxidative stress, we assayed the levels of MDA and SOD in the brain tissue of rats. As showed in Figure 4A, the level of MDA was increased in

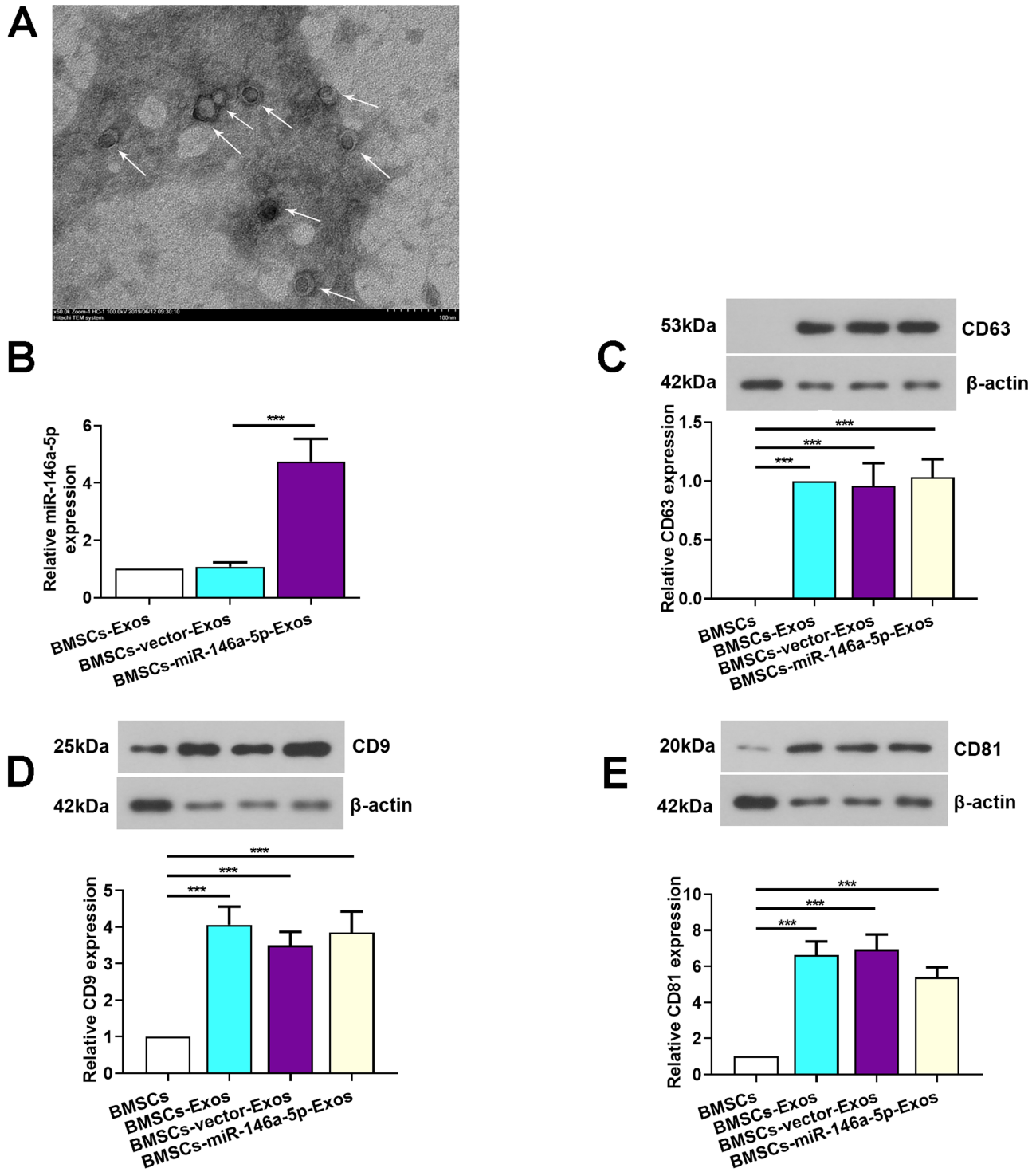

Figure 2 Characterization of Exos. (**A**) Representative electron microscopy image of Exos derived from BMSCs. (**B**) Expression level of miR-146a-5p in Exos. (**C**) Expression level of CD63 protein. (**D**) Expression level of CD9 protein. (**E**) Expression level of CD81 protein. The data are presented as the mean ± SD, ***p < 0.001.

the ICH group while significantly decreased in the Exos treatment group. In addition, the level of SOD was measured to determine the antioxidant condition in the brain. The results showed that the level of SOD significantly decreased in the ICH group while increased in the Exos treatment group (Figure 4B). Especially, miR-146a-5p-enriched Exos derived from BMSCs has stronger protective effects than BMSCs-Exos.

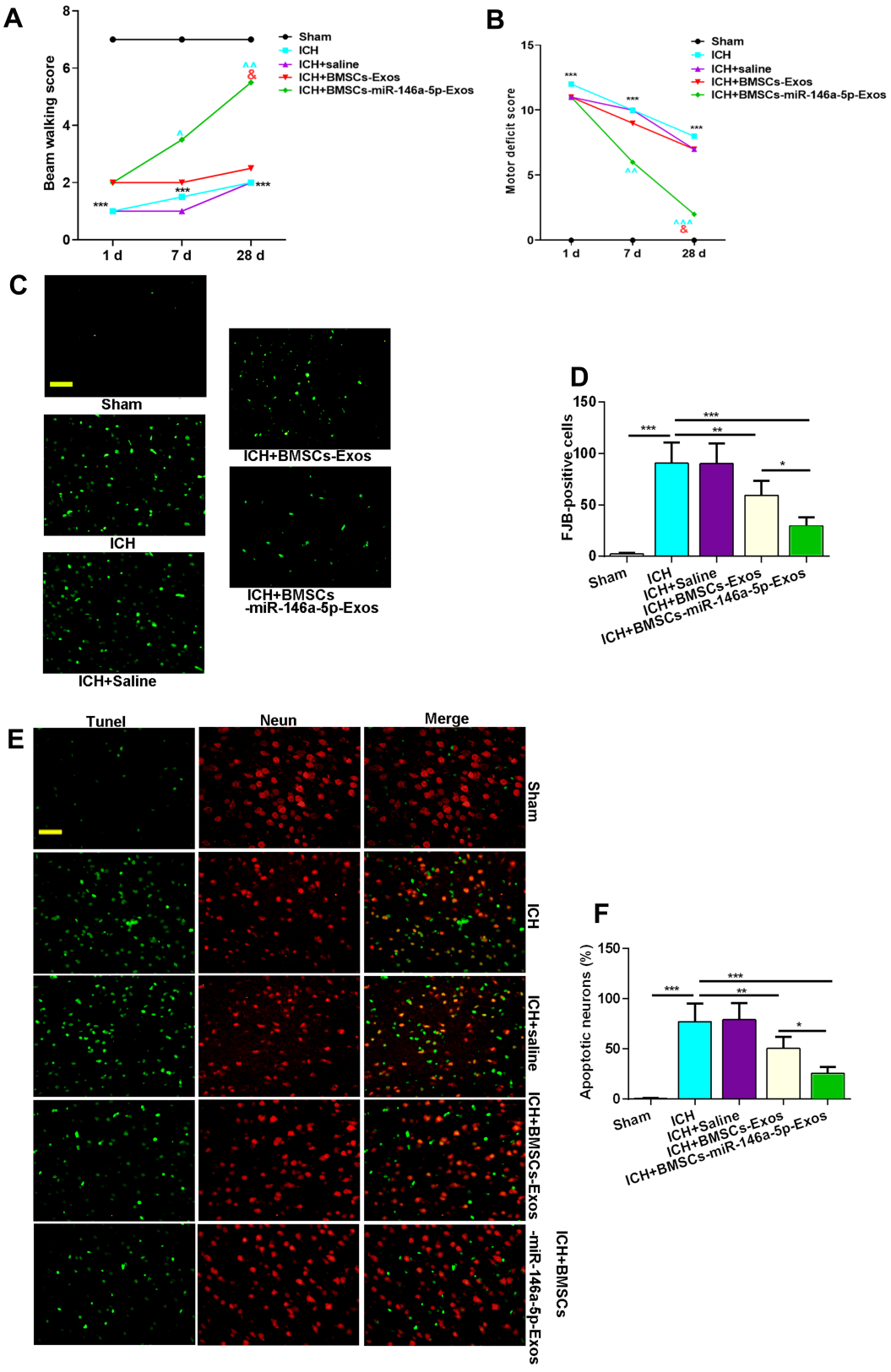

Figure 3 Effect of BMSCs-miR-146a-5p-Exos on nerve injuries in rats with ICH. (**A**) Beam-walking score. (**B**) Motor deficit score. (**C** and **D**) Representative photographs and quantification of degenerating neurons labeled with FJB in the brain tissues. (**E** and **F**) Representative photographs and quantification of apoptotic neurons labeled with TUNEL and NeuN in the brain tissues. The data for the motor deficit scores and the beam-walking tests are presented as median from twelve rats in each group, ***p< 0.001 compared with Sham group, ^p < 0.05 compared with ICH group, ^^p < 0.01 compared with ICH group, ^^^p < 0.001 compared with ICH group, &p < 0.05 compared with ICH + BMSCs-Exos group. The data for degenerating neurons and apoptotic neurons are presented as mean±SD from six rats in each group, *p < 0.05, **p < 0.01, ***p < 0.001, scale bar=50 μm.

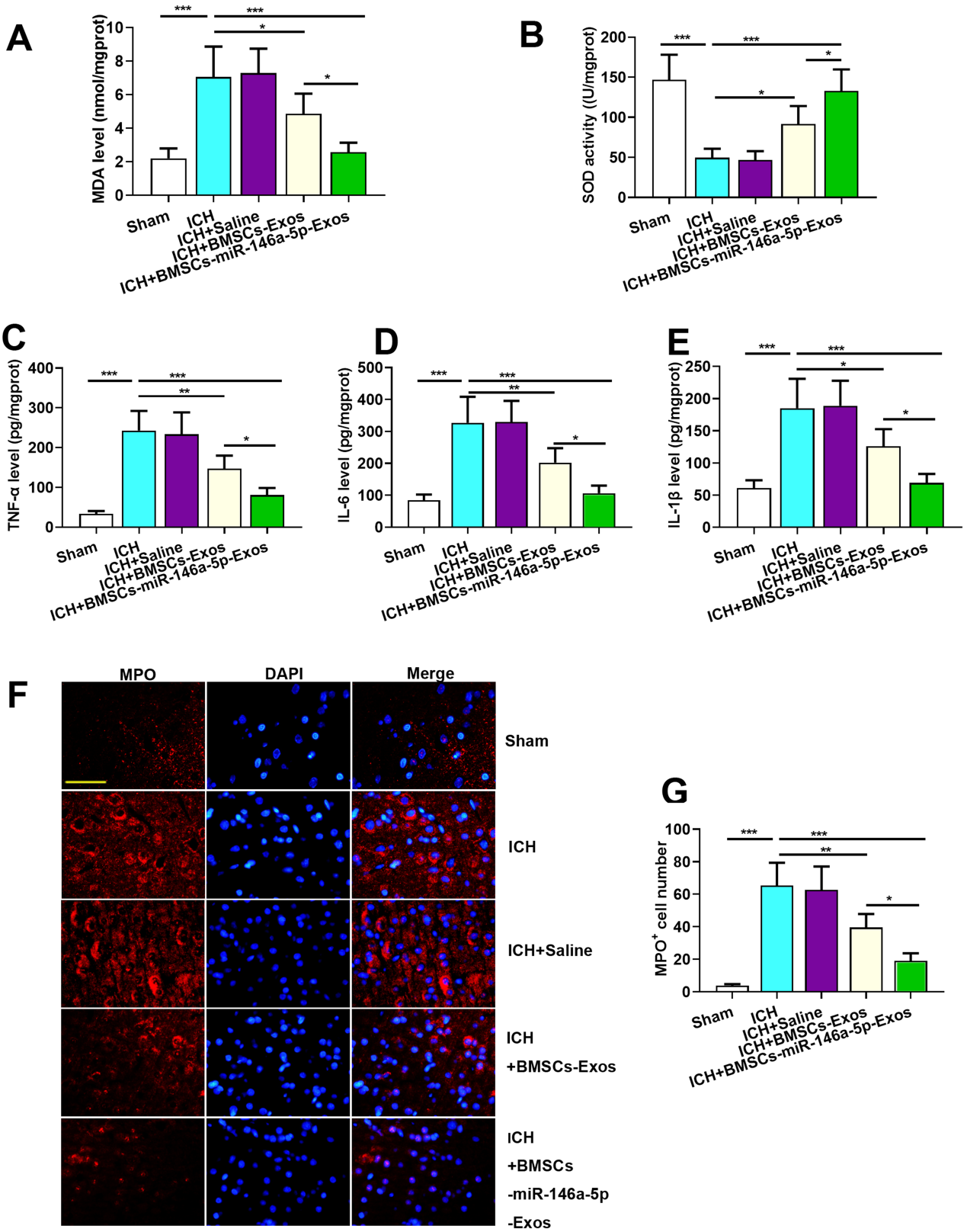

Figure 4 Effect of BMSCs-miR-146a-5p-Exos on oxidative stress and inflammation in the injured brain region of rats with ICH. (**A**) The level of MDA. (**B**) The activity of SOD. (**C**) The level of TNF-α. (**D**) The level of IL-6. (**E**) The level of L-1β. (**F**) Representative images of cells immunostained for MPO. (**G**) The number of MPO-positive cells. The data are presented as the mean ± SD from six rats in each group, *p < 0.05, **p < 0.01, ***p < 0.001, scale bar=50 μm.

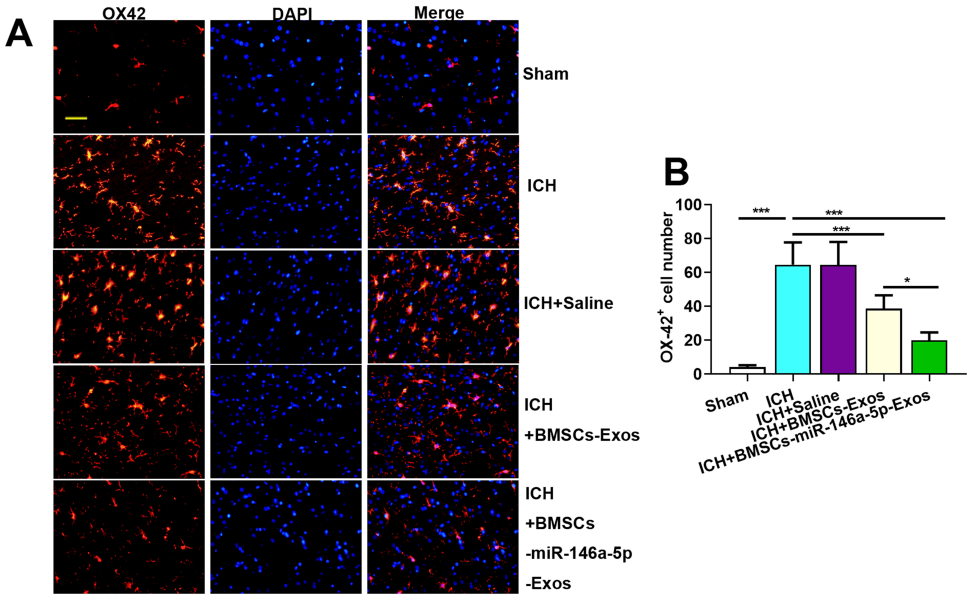

Figure 5 Effect of BMSCs-miR-146a-5p-Exos on microglial activation in the injured brain region of rats with ICH. (**A**) Representative images of cells immunostained for OX42. (**B**) The number of OX42-positive cells. The data are presented as the mean ± SD from six rats in each group, *p < 0.05, ***p < 0.001, scale bar=50 μm.

Given that ICH triggered inflammation response, we examined the effect of BMSCs-miR-146a-5p-Exos on inflammation post-ICH. The levels of inflammatory cytokines TNF-α, IL-1β, and IL-6 in the injured brain region of ICH rats were examined. As shown in Figure 4C–E, the levels of TNF-α, IL-1β, and IL-6 were significantly increased in the injured brain tissue of rats subjected to ICH, while these factors could be down-regulated by miR-146a-5p-enriched Exos. MPO, a marker of tissue neutrophil infiltration was measured to further confirm the inflammatory state. MPO-positive cells were abundant in the injured brain region of ICH rats, while BMSCs-miR-146a-5p-Exos administration obviously reduced the number of MPO-positive cells. BMSCs-miR-146a-5p-Exos exerted stronger effects on inflammation than BMSCs-Exos (Figure 4F and G).

Effect of BMSCs-MiR-146a-5p-Exos on Microglial Activation Following ICH

Given the important role of microglial activation in neuroinflammation, we next examined a marker of activated microglia OX42 in the injured brain region of ICH rats by immunohistochemistry assay. As shown in Figure 5A and B, ICH caused a remarkable elevation of OX42-positive cells, which was significantly attenuated by BMSCs-Exos, particularly by BMSCs-miR-146a-5p-Exos.

Effect of BMSCs-MiR-146a-5p-Exos on Microglial M1 Polarization Following ICH

Immunofluorescence staining for Iba-1 (microglia marker) and MHC-II (M1 marker) were performed to investigate the effects of BMSCs-miR-146a-5p-Exos on the microglial M1polarization. Results showed that ICH significantly increased the number of Iba-1^+/MHC-II^+ cells, while BMSCs-miR-146a-5p-Exos significantly reduced the number of Iba-1^+/MHC-II^+ cells (Figure 6A). Moreover, M1 microglia markers, including iNOS, COX2 and MCP-1 mRNA levels, were significantly elevated in the injured brain tissue of ICH rats. BMSCs-miR-146a-5p-Exos treatment could effectively reduce the levels of these M1 microglia markers (Figure 6B–D). Further, BMSCs-miR-146a-5p-Exos exerted a stronger inhibitory effect on M1 polarization of microglia than BMSCs-Exos.

MiR-146a-5p Derived from BMSC-Exos Alleviated ICH in Rats by Targeting IRAK1 and NFAT5

The expression level of miR-146a-5p was evaluated using qRT-PCR to further explore its neuroprotection. MiR-146a-5p expression level was significantly downregulated in ICH rats, while BMSCs-Exos administration slightly improved the level of miR-146a-5p. In addition, the miR-146a-5p

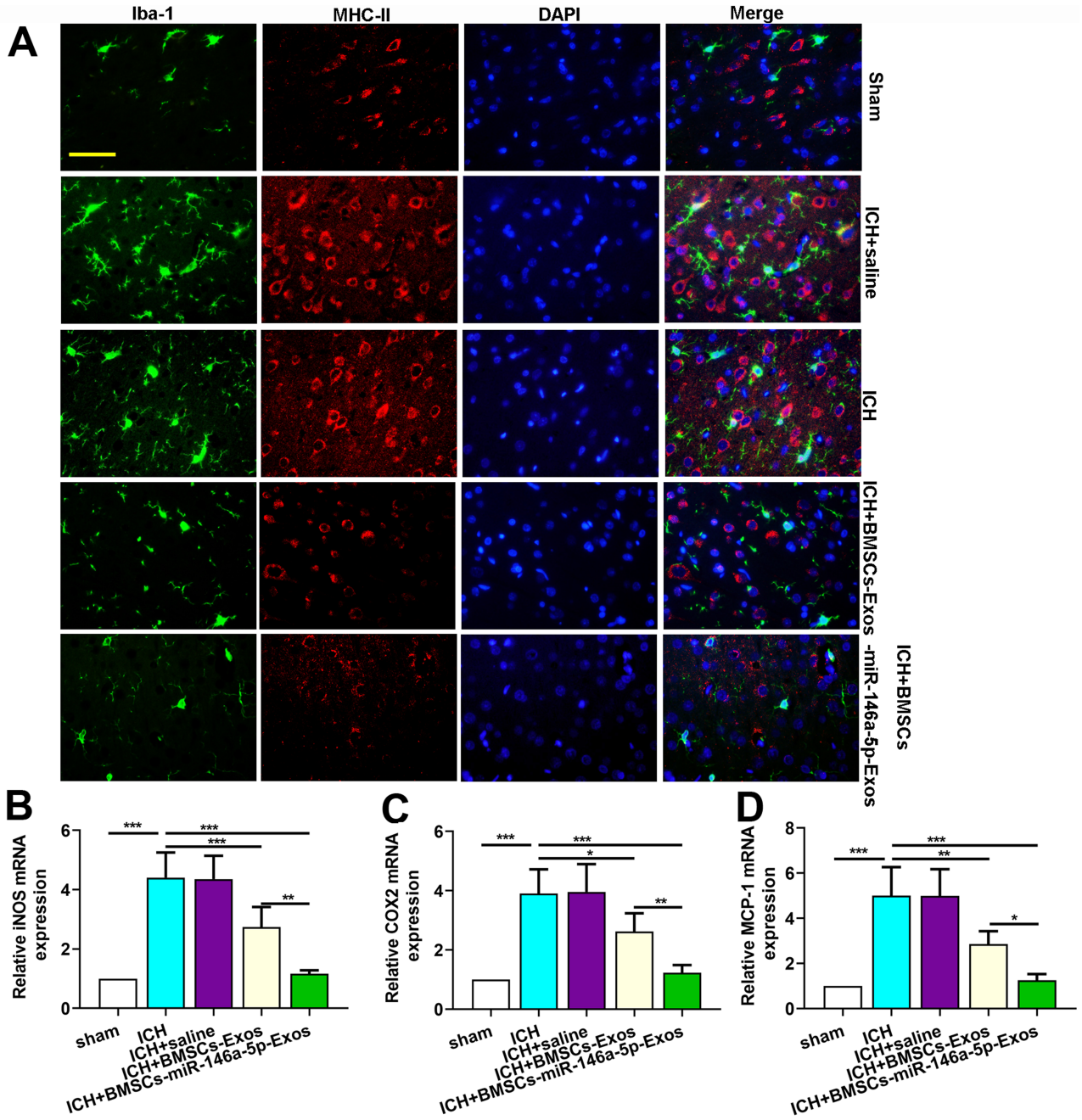

Figure 6 Effect of BMSCs-miR-146a-5p-Exos on microglial M1 polarization in the injured brain region after ICH. (**A**) Representative images of cells immunostained for Iba-1 and M1 marker MHC II. (**B**) The level of iNOS mRNA. (**C**) The level of COX2 mRNA. (**D**) The level of MCP-1 mRNA. The data are presented as the mean ± SD from six rats in each group, *p < 0.05, **p < 0.01, ***p < 0.001, scale bar=50 μm.

level was significantly higher in the BMSCs-miR-146a-5p-Exos group than that in the ICH and BMSCs-Exos group (Figure 7A).

To explore the potential mechanism of miR-146a-5p in alleviating ICH, we screened target genes IRAK1 and NFAT5 that were regulated by miR-146a-5p and were crucial for inflammation. We observed that the levels of IRAK1 and NFAT5 were increased after ICH induction compared with the Sham group, while miR-146a-5p-enriched Exos treatment exhibited a significant decrease in the IRAK1 (Figure 7B) and NFAT5 (Figure 7C) protein levels. Using luciferase reporter assay, we identified IRAK1 and NFAT5 as target genes of miR-146a-5p, as evidenced by suppression of their luciferase activities in the presence of miR-146a-5p. In contrast, mutation of the binding sites in the 3′-UTR of IRAK1 and NFAT5 prevented the inhibition

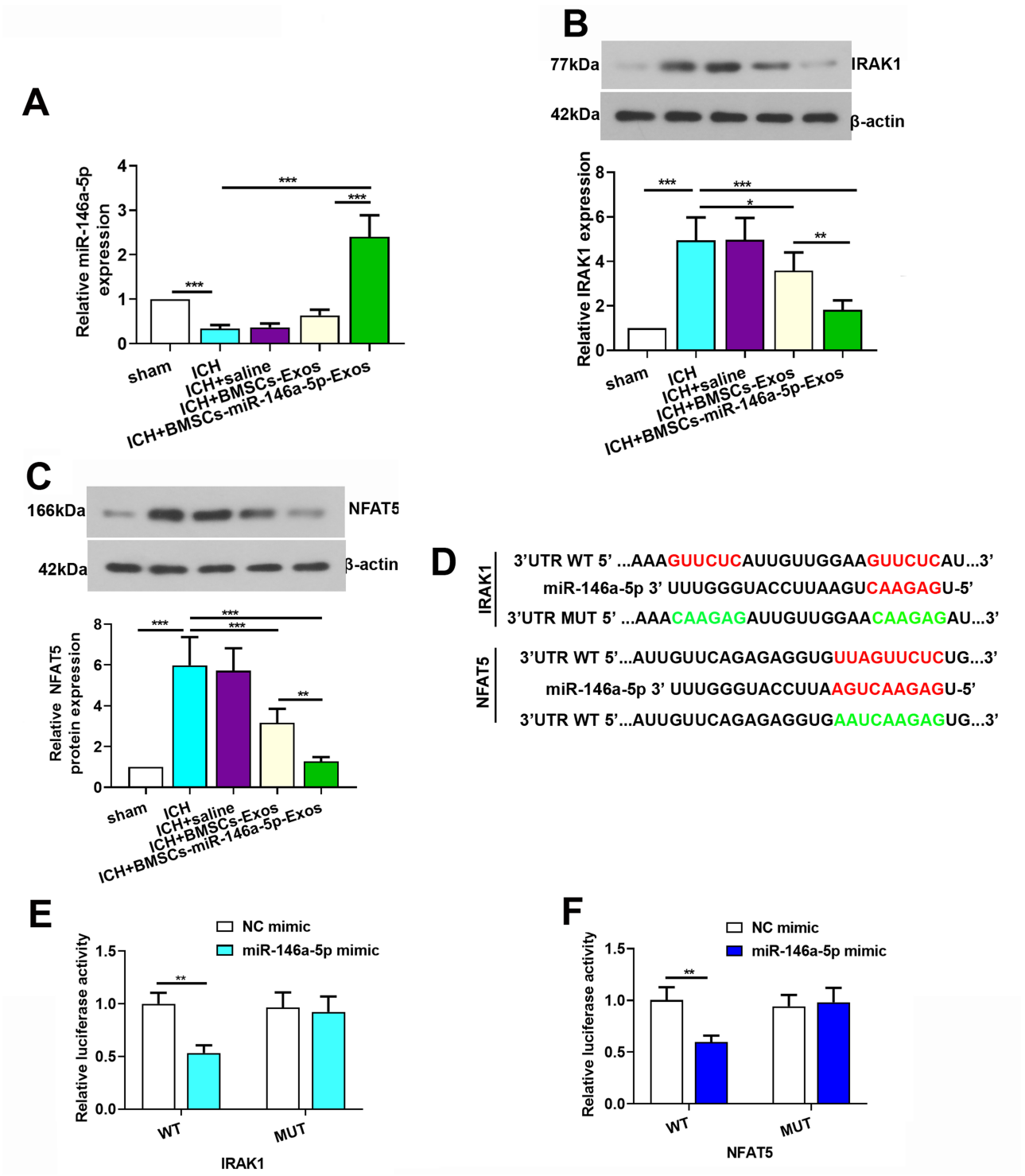

Figure 7 IRAK1 and NFAT5 were target genes of miR-146a-5p. (**A**) Expression level of miR-146a-5p in the brain tissue of rats. (**B** and **C**) Expression level of IRAK1 and NFAT5 protein in the brain tissue of rats. (**D**) A photograph depicted targeting sites of miR-146a-5p on IRAK1 and NFAT5 mRNA. (**E** and **F**) Dual-luciferase assay was performed to test binding between miR-146a-5p/IRAK1 and miR-146a-5p/NFAT5. The data for the expression of miR-146a-5p, IRAK1 and NFAT5 protein were derived from six rats in each group. The data are presented as the mean ± SD, *p < 0.05, **p < 0.01, ***p < 0.001.

of luciferase activity by miR-146a-5p (Figure 7D–F). These data confirm IRAK1 and NFAT5 as targets of miR-146a-5p. Additionally, we detected that microtubule-associated protein 1b (MAP1B) and p21-activated kinase 3 (PAK3) which were noted to regulate synaptic functions were also targets of miR-146a-5p (Supplemental Figure S2).

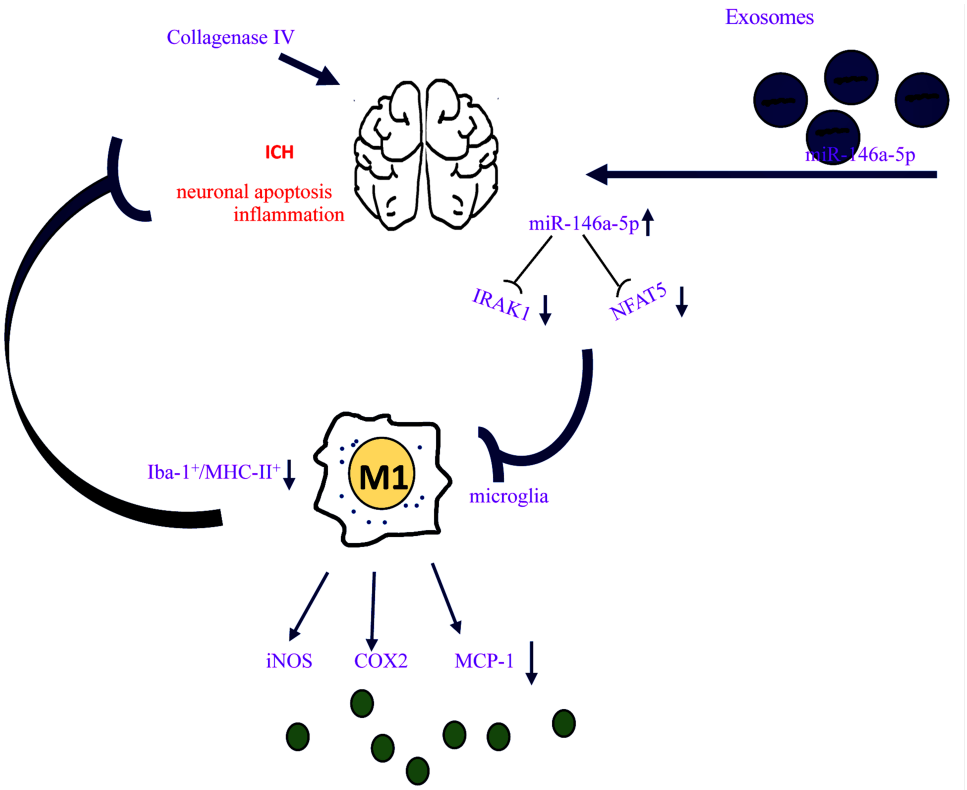

Figure 8 Schematic diagram of BMSCs-miR-146a-5p-Exos effect on brain damage post ICH. Exos derived from BMSCs loaded with miR-146a-5p could effectively alleviate brain injuries post ICH by reducing neuronal apoptosis and inflammation. BMSCs-miR-146a-5p-Exos exerts its anti-inflammation by inhibiting the M1 polarization of microglia thereby reducing the levels of pro-inflammatory factors including iNOS, COX2 and MCP-1 secreted by M1 microglia. Molecular mechanism of BMSCs-miR-146a-5p-Exos alleviating ICH may be associated with the inhibition of the expression of IRAK1 and NFAT5.

Discussion

Increased understanding of the important effect of cells that secrete a range of bioactive molecules has revealed a potential therapy for neurological disorders. BMSCs-based therapies have been reported in hypoxic brain injury,[26] traumatic brain injury[27] and ICH.[22,28] The release of neurotrophic factors by BMSCs in a paracrine manner has been considered to be a key mechanism of affecting physiological state of target tissues. Exos secreted by BMSCs were reported to mediate cell-to-cell communication, signaling pathway activation and decomposition of harmful substances, which may be involved in neuroprotective function.[29,30] MiR-enriched exosomes which are subsequently taken up by target cells could alter gene expression to exert biological functions.[31] The present study demonstrated that Exos derived from BMSCs loaded with miR-146a-5p could effectively alleviate brain injuries post ICH by reducing neuronal apoptosis, and inflammation associated with the suppression of microglial M1 polarization. Mechanism of BMSCs-miR-146a-5p-Exos alleviating ICH may be associated with the inhibition of the expression of IRAK1 and NFAT5 (Figure 8).

BMSCs-miR-146a-5p-Exos improved neurological function and reduced neuronal apoptosis post ICH in rats. MiRNAs, important components of the noncoding RNA family, regulate physiological and pathological processes.[32] Additionally, Exos are responsible for the delivery of miRNAs to the central nervous system, because of their stability and higher transfection efficiency.[33] In the present study, we focused our attention on the potential effects of Exos-transferred miR-146a-5p, and the possible molecular mechanisms involved in this process. Lentivirus infection was successfully performed in BMSCs which were isolated from rats to overexpress miR-146a-5p. As expected, the miR-146a-5p level was significantly increased both in BMSCs and Exos derived from BMSCs. Recent emerging evidences have indicated that BMSC-derived Exos containing miRs exert neuroprotective functions.[34,35] For example, BMSC-derived Exos containing overexpressed miR-138-5p reduce neurological impairment by inhibiting inflammatory response of astrocytes in ischemic stroke.[35] In another study, miR-21-overexpressing BMSCs inhibit neuronal death from secondary injury after ICH, which is mediated by miR-21

derived from exosomes.[34] Our results agreed well with the recent researches, Exos delivered miR-146a-5p to relieve neuromotor deficits, neuronal apoptosis and neurodegeneration post ICH. In addition, BMSCs-Exos also brought benefits to ICH, and miR-146a-5p-modified Exos obviously enhanced these protective effects. According to the previous researches, miR-146a-5p was abundant in MSCs and serves as a potential functional miR carried by MSC-Exos.[15,16] It was convincing that BMSCs-Exos had the potential to inhibit ICH partly related to the enriched miR-146a-5p expression in the BMSCs-Exos.

BMSCs-miR-146a-5p-Exos effectively suppressed inflammatory responses and microglial M1 polarization post ICH in rats. Oxidative stress and inflammation and are well recognized as risk factors for ICH-induced brain injury.[36,37] In terms of miR-146a-5p-enriched Exos on the impact of oxidative stress, we investigated the levels of MDA and SOD, which are primarily oxidative stress parameters. MiR-146a-5p-enriched Exos injection significantly reduces oxidative stress imbalance and the levels of pro-inflammatory factors in rats with ICH. As neuroinflammation is inevitable among most neurological disorders, MPO which is a marker of neutrophil infiltration is often measured to reflect neuroinflammation states.[38] The number of MPO-positive cells was significantly reduced by miR-146a-5p-enriched Exos. All these data indicated the anti-inflammation effect of BMSCs-miR-146a-5p-Exos in the brain of ICH rats. Microglia are resident macrophage-like cells of the central nervous system. Under normal physiological conditions, microglia contribute to maintaining tissue homeostasis and brain development. However, excessive microglial activation caused neuroinflammation and neuronal damage, and the factors secreted by the injured or dying neurons in turn exacerbate microglia activation.[39] Based on these, we hypothesized that microglia activation may be involved in the mechanism of BMSCs-miR-146a-5p-Exos alleviating ICH. OX-42 is a specific marker of activated microglia. Treatment with BMSCs-miR-146a-5p-Exos obviously reduced the number of OX42-positive cells which were abundant in the perihematomal region post ICH, confirming our hypothesis. The activation of microglial M1 polarization phenotype aggravates ICH-induced brain injury via the release of pro-inflammatory mediators. To further support our conjecture, the microglial marker Iba-1 and M1 phenotype marker MHC-II were simultaneously immunostained. ICH significantly increased while BMSCs-miR-146a-5p-Exos significantly reduced the number of Iba-1^{+}/MHC-II^{+} cells. Moreover, the mRNA level of M1 microglia markers, including iNOS, COX2 and MCP-1, were also significantly decreased with BMSCs-miR-146a-5p-Exos administration. These results supported that BMSCs-miR-146a-5p-Exos reduced inflammatory responses associated with the inhibition of microglia M1 polarization in ICH.

MiR-146a-5p delivering by BMSC-Exos alleviated ICH in rats by targeting IRAK1 and NFAT5. MiRNAs were transferred between cells to regulate the biological functions of recipient cells via inhibiting their target genes. We further explored possible mechanisms of miR-146a-5p transmitted by Exos inhibiting the process of ICH. The results showed that ICH was accompanied by decreased expression of miR-146a-5p, while it was highly expressed in the injured brain tissues after ICH transported by Exos. We then identified two critical miR-146a-5p targets upregulated after ICH with pro-inflammatory and macrophages/microglia polarization-modulated properties: IRAK1 and NFAT5.[40,41] IRAK1 is a kinase that belongs to interleukin-1 receptor-associated kinase (IRAK) family, mediating inflammatory responses in multiple pathological processes.[42] It contributes to the activation of NF-κB signaling pathway which is a well-known inflammation signaling pathway. MiR-146a-5p targeted IRAK1 inhibiting microglia M1 polarization in ICH echo findings from a previous study.[41] NFAT5, a novel member of Rel homology domain (RHD) proteins (Rel family), plays different roles in neurons, astrocytes, microglia, and other cell types in the central nervous system.[43,44] A number of studies suggest that NFAT5 can be activated by inflammatory stimuli induction and participates in neuroinflammation.[45,46] Furthermore, NFAT5 increased the expression of the M1-polarized macrophages characteristic genes to support the pro-inflammatory function of macrophages.[40] Thus, miR-146a-5p alleviated ICH-induced brain injury, potentially via direct inhibition of NFAT5. Herein, we provided molecular mechanisms responsible for miR-146a-5p modulating microglial M1 polarization (neuroinflammation). However, the limitation exists in this study, microglial M2 polarization was not evaluated. It has been reported that downregulating the expression of IRAK1 by miR-146a increases M2 polarization in BV-2 cells.[41] In another study, NFAT5 suppresses the macrophage M2 phenotype.[47] Thus, it can be assumed that BMSCs-miR-146a-5p-Exos administration elevates microglial M2 polarization by suppressing the expression of IRAK1 and NFAT5. The related M2 polarization will be studied in the future investigations.

Conclusions

Our study implies that miR-146a-5p-riched Exos released from BMSCs could offer neuroprotection and functional improvements after ICH through reducing neuronal apoptosis, and inflammation associated with the suppression of microglial M1 polarization by downregulating the expression of IRAK1 and NFAT5.

Ethics Approval

The study protocol was approved by the ethics committee of the First Affiliated Hospital of Harbin Medical University. All animal experiments were performed in accordance with the Guideline for the Care and Use of Laboratory Animals published by the National Institutes of Health.

Author Contributions

Shurong Duan: Conceptualization, Roles/Writing-original draft, and Project administration; Fei Wang: Visualization, Software; Jingwei Cao: Data curation, Software; Chunyan Wang: Conceptualization, Project administration, Writing-review and editing.

All authors contributed to data analysis, drafting or revising the article, gave final approval of the version to be published, and agree to be accountable for all aspects of the work.

Funding

This study was supported by grants from the National Natural Science Foundation of China (No. 81601063), the Doctoral Foundation of the First Affiliated Hospital of Harbin Medical University (No. 2017B015), the Post-doctoral Science Foundation of China (No. 2016M591550), and the Post-doctoral Science Foundation of Heilongjiang Province (No. LBH-Z16117).

Disclosure

The authors have no conflicts of interest to declare.

References

1. Xi G, Keep RF, Hoff JT. Mechanisms of brain injury after intracerebral haemorrhage. *Lancet Neurol*. 2006;5(1):53–63. doi:10.1016/S1474-4422(05)70283-0
2. Qureshi AI, Tuhrim S, Broderick JP, Batjer HH, Hondo H, Hanley DF. Spontaneous intracerebral hemorrhage. *N Engl J Med*. 2001;344(19):1450–1460. doi:10.1056/NEJM200105103441907
3. Ginhoux F, Lim S, Hoeffel G, Low D, Huber T. Origin and differentiation of microglia. *Front Cell Neurosci*. 2013;7:45. doi:10.3389/fncel.2013.00045
4. Su P, Zhang J, Wang D, et al. The role of autophagy in modulation of neuroinflammation in microglia. *Neuroscience*. 2016;319:155–167. doi:10.1016/j.neuroscience.2016.01.035
5. Sominsky L, De Luca S, Spencer SJ. Microglia: key players in neurodevelopment and neuronal plasticity. *Int J Biochem Cell Biol*. 2018;94:56–60. doi:10.1016/j.biocel.2017.11.012
6. Franco R, Fernández-Suárez D. Alternatively activated microglia and macrophages in the central nervous system. *Prog Neurobiol*. 2015;131:65–86. doi:10.1016/j.pneurobio.2015.05.003
7. Lan X, Han X, Li Q, et al. Pinocembrin protects hemorrhagic brain primarily by inhibiting toll-like receptor 4 and reducing M1 phenotype microglia. *Brain Behav Immun*. 2017;61:326–339. doi:10.1016/j.bbi.2016.12.012
8. Wan S, Cheng Y, Jin H, et al. Microglia activation and polarization after intracerebral hemorrhage in mice: the role of protease-activated receptor-1. *Transl Stroke Res*. 2016;7(6):478–487. doi:10.1007/s12975-016-0472-8
9. Gurunathan S, Kang MH, Jeyaraj M, Qasim M, Kim JH. Review of the isolation, characterization, biological function, and multifarious therapeutic approaches of exosomes. *Cells*. 2019;8(4):307. doi:10.3390/cells8040307
10. Wang Y, Zhao R, Liu D, Deng W. Exosomes derived from miR-214-enriched bone marrow-derived mesenchymal stem cells regulate oxidative damage in cardiac stem cells by targeting CaMKII. *Oxid Med Cell Longev*. 2018;2018:4971261.
11. Xiao Y, Geng F, Wang G. Bone marrow-derived mesenchymal stem cells-derived exosomes prevent oligodendrocyte apoptosis through exosomal miR-134 by targeting caspase-8. *J Cell Biochem*. 2018;6.
12. Otero-Ortega L, Gomez de Frutos MC, Laso-Garcia F, et al. Exosomes promote restoration after an experimental animal model of intracerebral hemorrhage. *J Cereb Blood Flow Metab*. 2018;38(5):767–779. doi:10.1177/0271678X17708917
13. Gareev I, Yang G, Sun J, et al. Circulating MicroRNAs as potential noninvasive biomarkers of spontaneous intracerebral hemorrhage. *World Neurosurg*. 2019.
14. Ouyang Y, Li D, Wang H, et al. MiR-21-5p/dual-specificity phosphatase 8 signalling mediates the anti-inflammatory effect of haem oxygenase-1 in aged intracerebral haemorrhage rats. *Aging Cell*. 2019;18(6):e13022.
15. Yang W, Zhang J, Xu B, et al. HucMSC-derived exosomes mitigate the age-related retardation of fertility in female mice. *Mol Ther*. 2020;28(4):1200–1213. doi:10.1016/j.ymthe.2020.02.003
16. Baglio SR, Rooijers K, Koppers-Lalic D, et al. Human bone marrow- and adipose-mesenchymal stem cells secrete exosomes enriched in distinctive miRNA and tRNA species. *Stem Cell Res Ther*. 2015;6(1):127. doi:10.1186/s13287-015-0116-z
17. Xie Y, Chu A, Feng Y, et al. MicroRNA-146a: a comprehensive indicator of inflammation and oxidative stress status induced in the brain of chronic T2DM rats. *Front Pharmacol*. 2018;9:478. doi:10.3389/fphar.2018.00478
18. Chu B, Zhou Y, Zhai H, Li L, Sun L, Li Y. The role of microRNA-146a in regulating the expression of IRAK1 in cerebral ischemia-reperfusion injury. *Can J Physiol Pharmacol*. 2018;96(6):611–617. doi:10.1139/cjpp-2017-0586
19. Qu X, Wang N, Cheng W, Xue Y, Chen W, Qi M. MicroRNA-146a protects against intracerebral hemorrhage by inhibiting inflammation and oxidative stress. *Exp Ther Med*. 2019;18(5):3920–3928. doi:10.3892/etm.2019.8060
20. Zhang H, Lu M, Zhang X, et al. Isosteviol sodium protects against ischemic stroke by modulating microglia/macrophage polarization via disruption of GAS5/miR-146a-5p sponge. *Sci Rep*. 2019;9(1):12221. doi:10.1038/s41598-019-48759-0
21. Hu YL, Wang H, Huang Q, Wang G, Zhang HB. MicroRNA-23a-3p promotes the perihematomal edema formation after intracerebral hemorrhage via ZO-1. *Eur Rev Med Pharmacol Sci*. 2018;22(9):2809–2816. doi:10.26355/eurrev_201805_14980

22. Wang C, Fei Y, Xu C, Zhao Y, Pan Y. Bone marrow mesenchymal stem cells ameliorate neurological deficits and blood-brain barrier dysfunction after intracerebral hemorrhage in spontaneously hypertensive rats. *Int J Clin Exp Pathol*. 2015;8(5):4715–4724.
23. Tsai MJ, Tsai SK, Hu BR, et al. Recovery of neurological function of ischemic stroke by application of conditioned medium of bone marrow mesenchymal stem cells derived from normal and cerebral ischemia rats. *J Biomed Sci*. 2014;21(1):5. doi:10.1186/1423-0127-21-5
24. Dominici M, Le Blanc K, Mueller I, et al. Minimal criteria for defining multipotent mesenchymal stromal cells. The international society for cellular therapy position statement. *Cytotherapy*. 2006;8(4):315–317. doi:10.1080/14653240600855905
25. Takamatsu Y, Tamakoshi K, Waseda Y, Ishida K. Running exercise enhances motor functional recovery with inhibition of dendritic regression in the motor cortex after collagenase-induced intracerebral hemorrhage in rats. *Behav Brain Res*. 2016;300:56–64. doi:10.1016/j.bbr.2015.12.003
26. Ali EHA, Ahmed-Farid OA, Osman AAE. Bone marrow-derived mesenchymal stem cells ameliorate sodium nitrite-induced hypoxic brain injury in a rat model. *Neural Regen Res*. 2017;12(12):1990–1999. doi:10.4103/1673-5374.221155
27. Hu J, Chen L, Huang X, et al. Calpain inhibitor MDL28170 improves the transplantation-mediated therapeutic effect of bone marrow-derived mesenchymal stem cells following traumatic brain injury. *Stem Cell Res Ther*. 2019;10(1):96. doi:10.1186/s13287-019-1210-4
28. Huang P, Freeman WD, Edenfield BH, Brott TG, Meschia JF, Zubair AC. Safety and efficacy of intraventricular delivery of bone marrow-derived mesenchymal stem cells in hemorrhagic stroke model. *Sci Rep*. 2019;9(1):5674.
29. Li C, Jiao G, Wu W, et al. Exosomes from bone marrow mesenchymal stem cells inhibit neuronal apoptosis and promote motor function recovery via the Wnt/beta-catenin signaling pathway. *Cell Transplant*. 2019;28(11):1373–1383.
30. Zhang Y, Chopp M, Zhang ZG, et al. Systemic administration of cell-free exosomes generated by human bone marrow derived mesenchymal stem cells cultured under 2D and 3D conditions improves functional recovery in rats after traumatic brain injury. *Neurochem Int*. 2017;111:69–81. doi:10.1016/j.neuint.2016.08.003
31. Indolfi C, Curcio A. Stargazing microRNA maps a new miR-21 star for cardiac hypertrophy. *J Clin Invest*. 2014;124(5):1896–1898. doi:10.1172/JCI75801
32. Rupaimoole R, Calin GA, Lopez-Berestein G, Sood AK. miRNA deregulation in cancer cells and the tumor microenvironment. *Cancer Discov*. 2016;6(3):235–246. doi:10.1158/2159-8290.CD-15-0893
33. Huang JH, Xu Y, Yin XM, Lin FY. Exosomes derived from miR-126-modified MSCs promote angiogenesis and neurogenesis and attenuate apoptosis after spinal cord injury in rats. *Neuroscience*. 2019.
34. Zhang H, Wang Y, Lv Q, Gao J, Hu L, He Z. MicroRNA-21 overexpression promotes the neuroprotective efficacy of mesenchymal stem cells for treatment of intracerebral hemorrhage. *Front Neurol*. 2018;9:931. doi:10.3389/fneur.2018.00931
35. Deng Y, Chen D, Gao F, et al. Exosomes derived from microRNA-138-5p-overexpressing bone marrow-derived mesenchymal stem cells confer neuroprotection to astrocytes following ischemic stroke via inhibition of LCN2. *J Biol Eng*. 2019;13(1):71. doi:10.1186/s13036-019-0193-0
36. Wang Z, Zhou F, Dou Y, et al. Melatonin alleviates intracerebral hemorrhage-induced secondary brain injury in rats via suppressing apoptosis, inflammation, oxidative stress, DNA damage, and mitochondria injury. *Transl Stroke Res*. 2018;9(1):74–91. doi:10.1007/s12975-017-0559-x
37. Zhou Y, Wang Y, Wang J, Anne Stetler R, Yang QW. Inflammation in intracerebral hemorrhage: from mechanisms to clinical translation. *Prog Neurobiol*. 2014;115:25–44. doi:10.1016/j.pneurobio.2013.11.003
38. Pravalika K, Sarmah D, Kaur H, et al. Myeloperoxidase and neurological disorder: a crosstalk. *ACS Chem Neurosci*. 2018;9(3):421–430.
39. Subhramanyam CS, Wang C, Hu Q, Dheen ST. Microglia-mediated neuroinflammation in neurodegenerative diseases. *Semin Cell Dev Biol*. 2019;94:112–120. doi:10.1016/j.semcdb.2019.05.004
40. Tellechea M, Buxade M. NFAT5-regulated macrophage polarization supports the proinflammatory function of macrophages and T lymphocytes. *J Immunol*. 2018;200(1):305–315.
41. Huang Y, Liao Z, Lin X, et al. Overexpression of miR-146a might regulate polarization transitions of BV-2 cells induced by high glucose and glucose fluctuations. *Front Endocrinol (Lausanne)*. 2019;10:719. doi:10.3389/fendo.2019.00719
42. Song T, Ma X, Gu K, et al. Thalidomide represses inflammatory response and reduces radiculopathic pain by inhibiting IRAK-1 and NF-kappaB/p38/JNK signaling. *J Neuroimmunol*. 2016;290:1–8. doi:10.1016/j.jneuroim.2015.11.007
43. Yi MH, Lee YS, Kang JW, et al. NFAT5-dependent expression of AQP4 in astrocytes. *Cell Mol Neurobiol*. 2013;33(2):223–232. doi:10.1007/s10571-012-9889-0
44. Yang XL, Wang X, Peng BW. NFAT5 has a job in the brain. *Dev Neurosci*. 2018;40(4):289–300. doi:10.1159/000493789
45. Jeong GR, Im SK, Bae YH, et al. Inflammatory signals induce the expression of tonicity-responsive enhancer binding protein (TonEBP) in microglia. *J Neuroimmunol*. 2016;295–296.
46. Wang R, Li Q, He Y, Yang Y, Ma Q, Li C. MiR-29c-3p inhibits microglial NLRP3 inflammasome activation by targeting NFAT5 in Parkinson's disease. *Genes Cells*. 2020;25(6):364–374. doi:10.1111/gtc.12764
47. Yoo EJ, Lee HH, Ye BJ, et al. TonEBP suppresses the HO-1 gene by blocking recruitment of Nrf2 to its promoter. *Front Immunol*. 2019;10:850. doi:10.3389/fimmu.2019.00850